J. Fluid Mech. (1982), *vol.* 114, *pp.* 299–314
Printed in Great Britain

Free-surface flow over a semicircular obstruction

By LAWRENCE K. FORBES AND LEONARD W. SCHWARTZ

Department of Applied Mathematics, University of Adelaide, South Australia 5000

(Received 12 September 1980 and in revised form 12 June 1981)

The two-dimensional steady flow of a fluid over a semicircular obstacle on the bottom of a stream is discussed. A linearized theory is presented, along with a numerical method for the solution of the fully nonlinear problem. The nonlinear free-surface profile is obtained after solution of an integrodifferential equation coupled with the dynamic free-surface condition. The wave resistance of the semicircle is calculated from knowledge of the solution at the free surface.

1. Introduction

In this paper, we consider the steady behaviour of an inviscid, incompressible fluid flowing in a horizontal stream, and disturbed by a semicircular obstacle lying on the bottom. The solution to such a problem is expected to provide at least qualitative insight into the mechanism of wave generation by submerged bodies moving beneath a free surface.

The motion of concentrated singularities beneath a free surface is an old problem in fluid mechanics, and is closely related to the topic of the present paper. Havelock (1927) calculated a linearized solution to the problem in which a dipole moves with constant velocity beneath the surface of an infinitely deep fluid at rest. He then assumed that, at some first order of approximation, his solution would also describe the flow about a circular cylinder beneath the surface of an infinitely deep fluid, as well as the flow about a semicircular obstruction on the bottom of a horizontal canal. Various other authors have presented similar linearized solutions to problems of this type. The book by Kochin, Kibel' & Roze (1964) contains detailed and elegant solutions for the cases of a point vortex, a point source and a dipole moving beneath the surface of an infinitely deep fluid. The corresponding solutions for a fluid of fixed finite depth are given in Wehausen & Laitone (1960) and Gazdar (1973).

The Havelock solution to the motion of a dipole beneath a free surface was reconsidered by Tuck (1965). He showed that the 'body' produced in the fluid by the dipole is in fact not closed, so that the front and back stagnation points lie on different streamlines. Thus a linearized solution to the present problem, to be discussed in § 3, will necessarily differ from Havelock's, since we shall require a closed body at all orders of approximation. In addition, Havelock's solution results in a dispersion relation which describes waves in an infinitely deep fluid, while the dispersion relation resulting from our linearized solution describes a fluid of finite depth. This fact is responsible for the existence of a second class of solutions to our problem, when the fluid flow is supercritical, which are symmetric about the semicircle and possess no waves.

Recently, a number of investigators have sought to retain the free-surface condition in its exact nonlinear form when dealing with problems of this type. Von Kerczek & Salvesen (1977) present a numerical solution to the two-dimensional steady problem in which waves are produced on the surface of a stream of finite depth by a given pressure distribution on the surface. The numerical method they employ is one which they have used successfully in the solution of similar problems, and consists of placing a finite-difference grid over the region of interest in the physical plane, and then iterating to find the location of the free surface such that all the flow equations and boundary conditions are satisfied. Haussling & Coleman (1977) describe the numerical solution of time-dependent potential flow problems of great generality by a boundary-fitting technique, in which a curvilinear co-ordinate system is generated numerically, so that lines in the new co-ordinate system correspond to physical boundaries. Shanks & Thompson (1977) show how this technique may be used to solve numerically free-surface problems in which time dependence and even viscosity are included.

In the present paper, we treat the physical co-ordinates, rather than the velocity potential and stream function, as the unknowns of the motion. Thus the location of the free surface in the inverse plane is now known. The bottom of the stream is transformed into a straight line using conformal mapping; consequently, an integral equation may be derived which involves values of the flow variables at the free surface only, with the bottom condition being satisfied automatically by reflection. Thus, points in the numerical scheme need only be placed at the free surface, rather than throughout the entire fluid. Details of this formulation are given in § 2. The linearized solution is presented in § 3, and our numerical scheme in § 4. Section 5 contains the results of numerical computations. Section 6 discusses the possible non-uniqueness of solutions for Froude numbers greater than one.

2. Formulation

We consider the steady, two-dimensional potential flow of an inviscid, incompressible fluid. Far upstream, the flow is uniform, with constant velocity c and fixed depth H. The fluid is subject to the downward acceleration of gravity g, and the radius of the disturbing semicircle is R.

The problem may immediately be non-dimensionalized with respect to the velocity c and depth H. The velocity potential ϕ and stream function ψ are normalized with respect to the product cH. The channel bottom is taken to be the $\psi = 0$ streamline, so that the free surface is $\psi = 1$. There is thus a two-parameter family of solutions to this problem, dependent upon the depth-based Froude number

$$F = \frac{c}{(gH)^{\frac{1}{2}}}$$

and the dimensionless circle radius

$$\alpha = \frac{R}{H}.$$

A sketch of the non-dimensional flow is given in figure 1.

The irrotationality and incompressibility of the fluid in the interior is expressed by the usual Cauchy–Riemann equations

$$\left.\begin{aligned} \phi_x &= \psi_y, \\ \phi_y &= -\psi_x, \end{aligned}\right\} \tag{2.1}$$

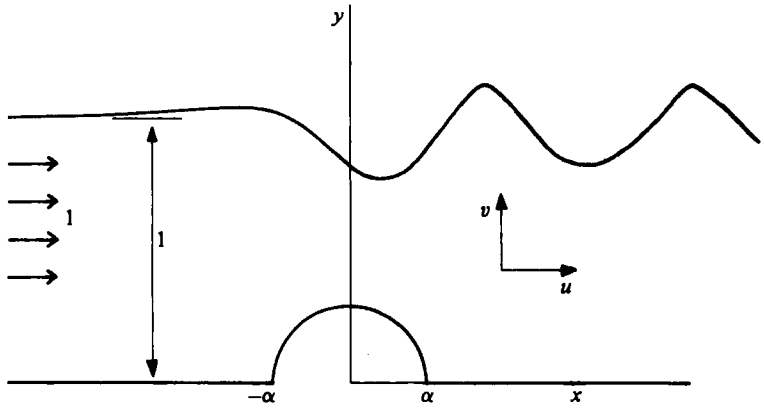

FIGURE 1. The non-dimensionalized problem and co-ordinate system.

where the subscripts denote partial differentiation. The condition of no flow normal to the bottom $y = h(x)$ may be written

$$uh_x = v \quad \text{at} \quad y = h(x), \tag{2.2}$$

where

$$h(x) = \begin{cases} (\alpha^2 - x^2)^{\frac{1}{2}} & (|x| \leqslant \alpha) \\ 0 & (|x| > \alpha) \end{cases}$$

and u and v are the horizontal and vertical components of velocity respectively. At the free surface of the fluid, we impose the Bernoulli equation

$$\tfrac{1}{2}F^2(u^2+v^2)+y = \tfrac{1}{2}F^2+1. \tag{2.3}$$

It is convenient at this stage to introduce the complex variables $z = x+iy$ and $f = \phi+i\psi$, and the conjugate complex velocity

$$w = \frac{df}{dz} = u-iv.$$

Now the solution of the above-stated problem can be greatly assisted by the choice of f as independent variable, rather than z. This choice, first suggested by Stokes (1880), has the obvious advantage of removing the difficulty associated with the free-surface condition, since, although the location of the surface is unknown in the z-plane, it has the *known* location $\psi = 1$ in the f-plane. However, we note that the Jacobian of the transformation from the z-plane to the f-plane becomes zero at the two stagnation points on the semicircle. These points would thus map into singularities in the f-plane. To avoid this, we first map the z-plane into a ζ-plane in which the bottom streamline is a straight line, free of singular points. The mapping required is the familiar Joukowski transformation

$$\zeta = \tfrac{1}{2}\left(z+\frac{\alpha^2}{z}\right),$$

where the new variable ζ is written as $\zeta = \xi+i\eta$. Figure 2 shows the mappings involved in the formulation of this problem.

By defining a new ζ-plane conjugate velocity

$$W = \frac{df}{d\zeta} = U-iV$$

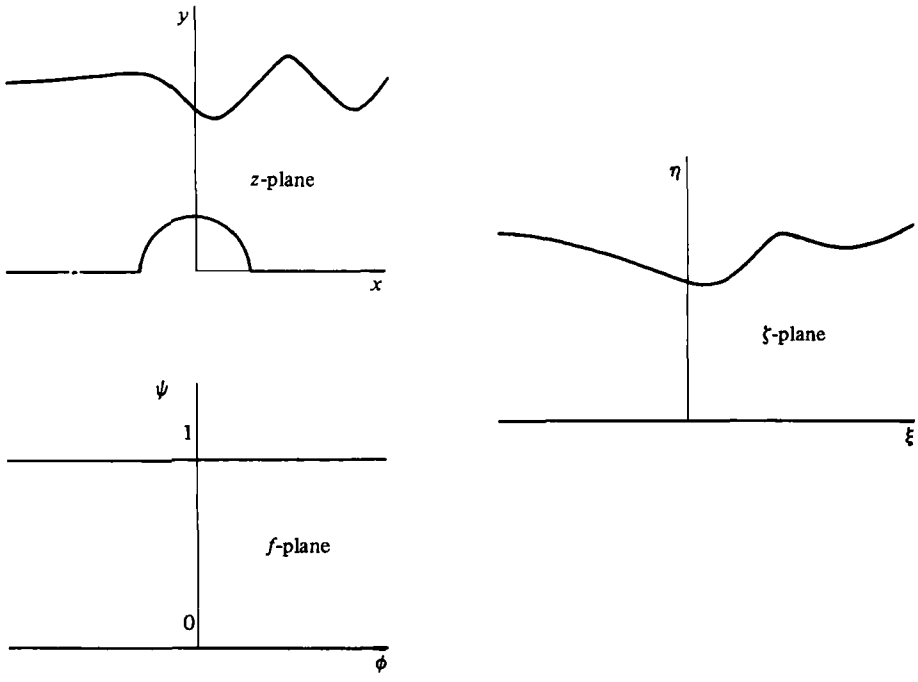

FIGURE 2. The various co-ordinate systems used in the formulation of the problem.

we may transform the z-plane equations (2.1)–(2.3) into the ζ-plane. Thus we seek an analytic function $f(\zeta)$ satisfying the bottom condition

$$V = 0 \quad \text{on} \quad \eta = 0,$$

and the appropriately transformed Bernoulli equation at the free surface.

As there are now no singular points either within the fluid or on the fluid boundaries in the ζ-plane, we may interchange the roles of ζ and f. In the f-plane, we seek an analytic function $\zeta(f)$ satisfying the bottom condition

$$\eta = 0 \quad \text{on} \quad \psi = 0. \tag{2.4}$$

The final form of the Bernoulli equation in the f-plane is

$$F^2 \frac{(z^2-\alpha^2)(\bar{z}^2-\alpha^2)}{8(z\bar{z})^2(\xi_\phi^2+\eta_\phi^2)} + \mathscr{S}\{z\} - 1 - \tfrac{1}{2}F^2 = 0 \quad \text{on} \quad \psi = 1, \tag{2.5}$$

where $z(\zeta)$ is found from

$$z = \zeta + (\zeta^2-\alpha^2)^{\frac{1}{2}}, \tag{2.6}$$

and the bars signify complex conjugation. The branch of the radical in (2.6) is chosen so that $z = 2\zeta$ when $\alpha = 0$.

We now derive an integral equation relating the real and imaginary parts of $\zeta'(f)$ along the free surface $\psi = 1$. Consider the function

$$\chi(f) = \frac{d\zeta}{df} - \tfrac{1}{2}.$$

This function is analytic in the f-plane strip $0 \leqslant \psi \leqslant 1$ and vanishes as $\phi \to -\infty$.

Far downstream, $\chi(f)$ is bounded and its mean value is zero. By the bottom condition (2.4), we have $\mathscr{I}\{\zeta'(f)\} = 0$ on $\psi = 0$; consequently the strip $0 \leqslant \psi \leqslant 1$ may be extended by reflection about $\psi = 0$ to form the augmented section $-1 \leqslant \psi \leqslant 1$. The bottom condition (2.4) then requires that values of ζ' on the image strip be related to values on the true strip by the formula

$$\zeta'(\bar{f}) = \bar{\zeta}'(f). \tag{2.7}$$

When Cauchy's integral theorem is applied to the function $\chi(f)$ on a rectangular path consisting of the free surface $\psi = 1$ and its image $\psi = -1$ connected by vertical lines at $\phi \to \pm\infty$, we obtain

$$\chi(f) = \frac{1}{2\pi i}\left\{-\int_{-\infty}^{\infty} \frac{\chi(\theta+i)\,d\theta}{\theta+i-f} + \int_{-\infty}^{\infty} \frac{\chi(\theta-i)\,d\theta}{\theta-i-f}\right\}, \tag{2.8}$$

for points $f = \phi + i\psi$ within the path of integration. We now let f become a point on the true free surface, so that $f = \phi + i$. The path of integration is as before, except that the point $f = \phi + i$ is bypassed by a semicircular path of vanishingly small radius. For points on the free surface, we have

$$\chi(\phi+i) = \frac{1}{\pi i}\left\{-\int_{-\infty}^{\infty} \frac{\chi(\theta+i)\,d\theta}{\theta-\phi} + \int_{-\infty}^{\infty} \frac{\chi(\theta-i)\,d\theta}{\theta-\phi-2i}\right\}. \tag{2.9}$$

The desired relation is obtained by taking the real part of (2.9), using (2.7) to eliminate quantities at the image free surface. This yields

$$\begin{aligned}[\xi_\phi(\phi,1)-\tfrac{1}{2}] - \frac{2}{\pi}\int_{-\infty}^{\infty} [\xi_\theta(\theta,1)-\tfrac{1}{2}]\,\frac{d\theta}{(\theta-\phi)^2+4} \\ = -\frac{1}{\pi}\left\{\int_{-\infty}^{\infty} \frac{\eta_\theta(\theta,1)\,d\theta}{\theta-\phi} + \int_{-\infty}^{\infty} \frac{\eta_\theta(\theta,1)\,(\theta-\phi)\,d\theta}{(\theta-\phi)^2+4}\right\}.\end{aligned} \tag{2.10}$$

The free-surface profile is thus obtained by solving the Bernoulli equation (2.5) coupled with (2.10) and subject to the radiation condition

$$\zeta \to \tfrac{1}{2}f \quad \text{as} \quad \phi \to -\infty. \tag{2.11}$$

Once the shape of the free surface has been determined, all other flow quantities may be obtained. Of particular interest is the wave drag D, which is the horizontal component of the force acting on unit width of the semicircular cylinder, made dimensionless by reference to the quantity $\rho g H^2$. Here ρ is the fluid density. We have

$$D = \int_{-\alpha}^{\alpha} ph'(x)\,dx = \tfrac{1}{2}F^2\int_{-\alpha}^{\alpha} (u^2+v^2)\,\frac{x}{(\alpha^2-x^2)^{\frac{1}{2}}}\,dx,$$

where p is the pressure on the surface of the semicircle (in units of $\rho g H$). Transforming this equation into the ζ-plane yields

$$D = \frac{F^2}{2\alpha^2}\int_{-\alpha}^{\alpha} U^2\xi(\alpha^2-\xi^2)^{\frac{1}{2}}\,d\xi, \tag{2.12}$$

which in the f-plane becomes

$$D = \frac{F^2}{2\alpha^2}\int_{\phi-\alpha}^{\phi+\alpha} \frac{\xi(\alpha^2-\xi^2)^{\frac{1}{2}}}{\xi_\phi}\,d\phi. \tag{2.13}$$

The quantities $\phi_{\pm\alpha}$ are the solutions to the equations

$$\xi(\phi_{\pm\alpha}, 0) = \pm\alpha. \tag{2.14}$$

3. The linearized solution

In this section, we derive an approximate solution to the equations of motion by assuming that the square of the circle radius, α^2, is a small quantity. This solution is in fact the first-order term in a regular series expansion in the parameter α^2; in principle, the series may be continued to any desired order, although the complexity of the equations to be solved becomes prohibitive for any order greater than the first.

We express the solution $\zeta(f)$ as the regular perturbation expansion

$$\zeta(f) = \tfrac{1}{2}f + \alpha^2\mathscr{F}_1(f) + O(\alpha^4), \tag{3.1}$$

and seek to determine the function $\mathscr{F}_1(f)$ in the form

$$\mathscr{F}_1(f) = \int_0^\infty C(\kappa)\sin\kappa f\, d\kappa. \tag{3.2}$$

We observe that equation (3.2) satisfies the bottom condition $\mathscr{I}\{\mathscr{F}_1\} = 0$ on $\psi = 0$. By applying the linearized free-surface condition

$$\mathscr{R}\left\{\frac{d\mathscr{F}_1}{df} + \frac{i}{F^2}\mathscr{F}_1\right\} = \frac{1}{2F^2(\phi^2+1)} + \frac{1-\phi^2}{2(\phi^2+1)^2} \quad \text{on} \quad \psi = 1, \tag{3.3}$$

the real function $C(\kappa)$ is determined to be

$$C(\kappa) = \frac{e^{-\kappa}(\kappa + 1/F^2)}{2(\kappa\cosh\kappa - 1/F^2\sinh\kappa)}.$$

The free-surface condition (3.3) and the assumed form of the solution (3.2) both require that the real and imaginary parts of the function $\mathscr{F}_1$ be odd and even functions of ϕ, respectively. However, this condition is only satisfied when $F^2 > 1$, since in this case the function $C(\kappa)$ is non-singular, and so the right-hand side of (3.2) is well-defined. A free-surface profile is predicted which is symmetric about $\phi = 0$ and possesses no waves.

For the critical case $F^2 = 1$, there is no solution, since $\mathscr{F}_1$ becomes unbounded due to a singularity in the function $C(\kappa)$ at $\kappa = 0$.

When $F^2 < 1$, the function $C(\kappa)$ possesses a singularity at $\kappa = \kappa_0$, where κ_0 is the positive real root of the dispersion relation

$$\tanh\kappa_0 = F^2\kappa_0,$$

and so the Fourier integral in (3.2) fails to exist in the usual sense. It is thus necessary to interpret (3.2) as a contour integral in the complex κ-plane, with the path of integration bypassing the pole singularity at κ_0 in a semicircular path of vanishingly small radius. In this case, the solution (3.1) becomes

$$\zeta(f) = \tfrac{1}{2}f + \tfrac{1}{2}\alpha^2\left\{\int_0^\infty \frac{e^{-\kappa}(\kappa+1/F^2)\sin\kappa f\, d\kappa}{\kappa\cosh\kappa - 1/F^2\sinh\kappa} + \frac{\pi e^{-\kappa_0}(\kappa_0+1/F^2)\cos\kappa_0 f}{(1-1/F^2+\kappa_0^2F^2)\cosh\kappa_0}\right\} + O(\alpha^4). \tag{3.4}$$

Far upstream, the two terms within the brackets in (3.4) cancel, so that the radiation condition (2.11) is satisfied. Far downstream, however, the terms within the brackets

reinforce, summing to twice the value of the second term. Thus the limiting form of (3.4) downstream is

$$\zeta(f) \to \tfrac{1}{2}f + \frac{A_1}{2\sinh\kappa_0}\cos\kappa_0 f + O(\alpha^4) \quad \text{as} \quad \phi \to +\infty, \tag{3.5}$$

where the wave amplitude A_1 is given by

$$A_1 = 2\alpha^2 \frac{\pi e^{-\kappa_0}(\kappa_0 + 1/F^2)\sinh\kappa_0}{(1 - 1/F^2 + \kappa_0^2 F^2)\cosh\kappa_0}. \tag{3.6}$$

The free-surface profile is obtained by setting $\psi = 1$ in (3.4) and then using (2.6) to obtain $z(\zeta)$. The surface possesses a regular wave train downstream of the bump, but is free of waves upstream. Far downstream, (3.5) yields the free-surface profile

$$y \to 1 - A_1 \sin\kappa_0 x + O(\alpha^4) \quad \text{as} \quad x \to +\infty.$$

Note that the wave amplitude A_1 defined by (3.6) is twice the value calculated by Lamb (1932, p. 410, equation (9)). Implicit in Lamb's solution is the assumption that the length of the disturbance on the bottom must be of the same order of magnitude as the undisturbed fluid depth; consequently, for a semicircular disturbance where this assumption is no longer valid, Lamb's theory ceases to apply.

The linearized wave drag D is calculated by inverting (3.4) to obtain a relation of the form $f = f(\zeta)$, and then substituting into (2.12) with $\eta = 0$ ($\psi = 0$). This results in the classical formula

$$D = \tfrac{1}{4}A_1^2\left[1 - \frac{2\kappa_0}{\sinh 2\kappa_0}\right], \tag{3.7}$$

which may be found in Lamb (1932, p. 415).

4. Numerical methods

This section describes the numerical scheme used to solve the nonlinear system (2.5), (2.10) and (2.11), at the $N+1$ equally spaced surface points $\phi_0, \phi_1, \ldots, \phi_N$. The quantities ϕ_0 and ϕ_N are chosen to represent $-\infty$ and $+\infty$, respectively.

The integrodifferential equation (2.10) is first truncated upstream and downstream at the points ϕ_0 and ϕ_N. The error introduced by this process will be discussed in § 5. Now the singularity is subtracted from the Cauchy principal value integral, leaving a non-singular integral plus a natural-logarithm term. We next wish to discretize this approximation to the original equation (2.10), but in a manner which allows us the freedom to specify conditions at the first point ϕ_0 in accordance with the radiation condition (2.11). This is achieved by evaluating the integrodifferential equation at the N mid-points $\phi_{k-\frac{1}{2}}$, $k = 1, \ldots, N$. After discretization, we obtain a matrix system of the form

$$[\xi'_{k-\frac{1}{2}} - \tfrac{1}{2}] - \frac{2}{\pi}\sum_{j=0}^{N} a_{kj}[\xi'_j - \tfrac{1}{2}] = -\frac{1}{\pi}\sum_{j=0}^{N} b_{kj}\eta'_j - \frac{1}{\pi}\eta'_{k-\frac{1}{2}}\log\frac{\phi_N - \phi_{k-\frac{1}{2}}}{\phi_{k-\frac{1}{2}} - \phi_0} \quad (k = 1, \ldots, N), \tag{4.1}$$

where the primes denote differentiation with respect to ϕ, along $\psi = 1$. The coefficients a_{kj} and b_{kj} are known functions of $\phi_{k-\frac{1}{2}}$ and ϕ_j, and depend upon the quadrature formula used to discretize the integrals. We have used Simpson's rule for this purpose. The quantities $\xi'_{k-\frac{1}{2}}$ and $\eta'_{k-\frac{1}{2}}$ are now written in terms of values of $\xi'(\phi, 1)$ and $\eta'(\phi, 1)$ at neighbouring whole points $\phi_{k-1}, \phi_k, \phi_{k+1}$ etc. by means of a three-point interpolation

formula. This interpolation formula must be chosen to be consistent with the parabolae fitted by the Simpson's rule integration used in obtaining (4.1), otherwise unacceptably large errors may result. Equation (4.1) becomes

$$\sum_{j=0}^{N} c_{kj}[\xi'_j - \tfrac{1}{2}] = \sum_{j=0}^{N} d_{kj}\eta'_j \quad (k = 1, \ldots, N). \tag{4.2}$$

If ξ'_0 and η'_0 are assumed known, (4.2) may be inverted to yield the solution

$$\xi'_i = \tfrac{1}{2} + \sum_{j=1}^{N} H_{ij}\eta'_j + H_{i,N+1}[\xi'_0 - \tfrac{1}{2}] + H_{i,N+2}\eta'_0 \quad (i = 1, \ldots, N). \tag{4.3}$$

In practice, we usually obtain η'_0, η_0 and ξ_0 from the linearized solution, and then calculate ξ'_0 from the Bernoulli equation (2.5) evaluated at the first point ϕ_0.

The vectors ξ_i and η_i are now obtained by numerical integration, using Gregory's correction to the trapezoidal rule. Thus

$$\left.\begin{aligned} \xi_i &= \xi_0 + \sum_{j=0}^{N} w_{ij}\xi'_j, \\ \eta_i &= \eta_0 + \sum_{j=0}^{N} w_{ij}\eta'_j \quad (i = 1, \ldots, N), \end{aligned}\right\} \tag{4.4}$$

where the w_{ij} are appropriate weights.

The Bernoulli equation (2.5) evaluated at each of the N points $\phi_1, \ldots, \phi_N$ yields a system of N nonlinear algebraic equations in the N unknowns $\eta'_1, \ldots, \eta'_N$, after the functions ξ', ξ and η have all been eliminated using (4.3) and (4.4). This system is then solved by a modified Newton iteration scheme. Denoting the pressure at the ith free-surface point by P_i, we seek to solve

$$P_i(\eta'_j) = 0 \quad (i, j = 1, \ldots, N).$$

We begin the iteration process with suitable estimates for the unknowns η'_j. These are usually provided by the linearized solution. The estimate $\eta'^{(k)}_j$ at the kth iteration is updated according to the formula

$$\eta'^{(k+1)}_j = \eta'^{(k)}_j + \Delta^{(k)}_j,$$

where the correction step $\Delta^{(k)}_j$ is the solution to the matrix equation

$$\sum_{j=1}^{N} \left[\frac{\partial P_i}{\partial \eta'_j}\right]^{(k)} \Delta^{(k)}_j = -P^{(k)}_i.$$

If at any iteration in the Newton process a worse estimate of the solution is obtained than before, in the sense that $P^{(k+1)}_{\text{rms}} > P^{(k)}_{\text{rms}}$, where P_{rms} is the root-mean-squared residual pressure

$$P_{\text{rms}} = \frac{1}{N}\left(\sum_{i=1}^{N} P_i^2\right)^{\frac{1}{2}},$$

then the correction step $\Delta^{(k)}_j$ is halved and the iteration is repeated.

The above scheme has usually been found to be quadratically convergent; typically, a converged solution with $P_{\text{rms}} < 10^{-10}$ is obtained from the linearized solution in five iterations. When 131 points are used, the process of obtaining the linearized solution and the converged nonlinear solution requires about three minutes of computing time on a CDC CYBER 173 machine.

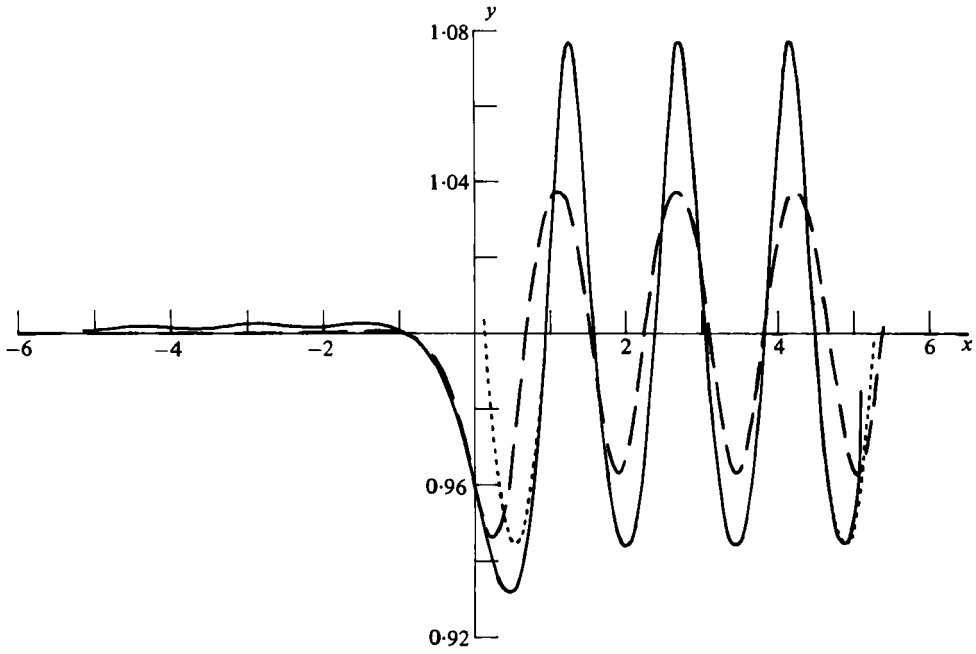

FIGURE 3. A comparison of the linearized (— —) and nonlinear (——) solutions to the problem for the case $F = 0{\cdot}5$, $\alpha = 0{\cdot}2$. A uniform train of Stokes waves (- - - - -) of the same phase and wave height as the downstream waves in the nonlinear solution is also shown.

For large values of the circle radius α, it is often not possible to obtain a converged nonlinear solution using the linearized results as an initial approximation in the Newton scheme. For these cases, a previously-computed nonlinear solution is used instead.

The wave drag D is computed from the converged nonlinear free-surface profile using (2.8) to generate values of ξ at points along the bottom $\psi = 0$. A cubic spline is then fitted through these points so that (2.14) may be solved for $\phi_{\pm\alpha}$ by Newton's method. Once these quantities are known, (2.13) is evaluated using the trapezoidal rule, since the integrand is well-behaved at all points within the range of integration.

5. Numerical results

5.1. *Subcritical case*, $F < 1$

In figure 3, we compare the linearized and nonlinear solutions for the case $F = 0{\cdot}5$, $\alpha = 0{\cdot}2$. The linearized free surface possesses a wave-free region upstream of the semicircular bump, followed by a regular wave train downstream. These general features are confirmed by the nonlinear result, although the amplitude of the nonlinear waves downstream is significantly greater. In addition, the nonlinear waves are noticeably non-sinusoidal, with narrow crests and broad troughs. The ratio of peak-to-trough amplitude to the wavelength (i.e. the steepness) is approximately 0·091. Since Newton's method fails to converge for larger values of the circle radius α, these are the steepest waves that we are presently able to compute at this value of the Froude number. By contrast, the steepness of the Stokes wave of maximum theoretical height

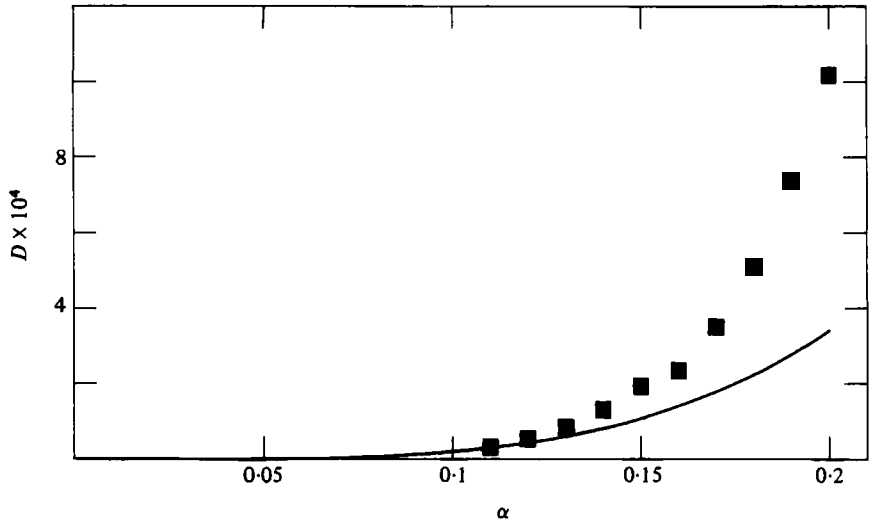

FIGURE 4. The dependence of wave drag upon α for the linearized (——) and nonlinear (■) solutions, when $F = 0{\cdot}5$.

at this Froude number is known to be approximately 0·14 (see, e.g. Cokelet 1977). This inability of our numerical method to compute very steep waves is a consequence of the relatively small number of free-surface points (about 20 points per wave cycle) to which we are restricted by the storage limits of the computer, and the inclusion of more points at the free surface would doubtless allow waves of much greater steepness to be obtained.

The corresponding nonlinear Stokes wave train for this value of the Froude number and wave height, computed by the numerical method of Schwartz & Vanden-Broeck (1979), is also shown in figure 3. The nonlinear result is virtually indistinguishable from the Stokes wave train, except within a distance of about half a wavelength downstream of the circle. A discrepancy also appears over the last quarter-wavelength downstream. This is a numerical error caused by the truncation of the integrodifferential equation (2.10) downstream at the last point ϕ_N.

On the other hand, the truncation of the integrodifferential equation upstream at the first point ϕ_0 has a more pronounced effect, being responsible for the generation of spurious waves of small amplitude in the upstream portion of the flow. Their amplitude, although small, can be altered by very small changes in the values of η_0, η_0' etc. imposed at the first point ϕ_0, while the downstream portion of the flow and the drag on the semicircle remain unchanged. The amplitude of the upstream waves in figure 3 has been reduced as far as possible by increasing the value of η_0 slightly above the value suggested by the linearized solution. A further reduction in the amplitude is to be expected by similarly varying the other flow quantities imposed at the point ϕ_0; this has not been pursued here, however, since each alteration to a flow quantity at ϕ_0 involves a full solution of the problem. In view of the physical implausibility of upstream waves in the present problem, the 'correct' conditions to be imposed at ϕ_0 can be defined as that choice which removes these spurious waves entirely.

Figure 4 shows the dependence of the wave drag D upon the circle radius α, for

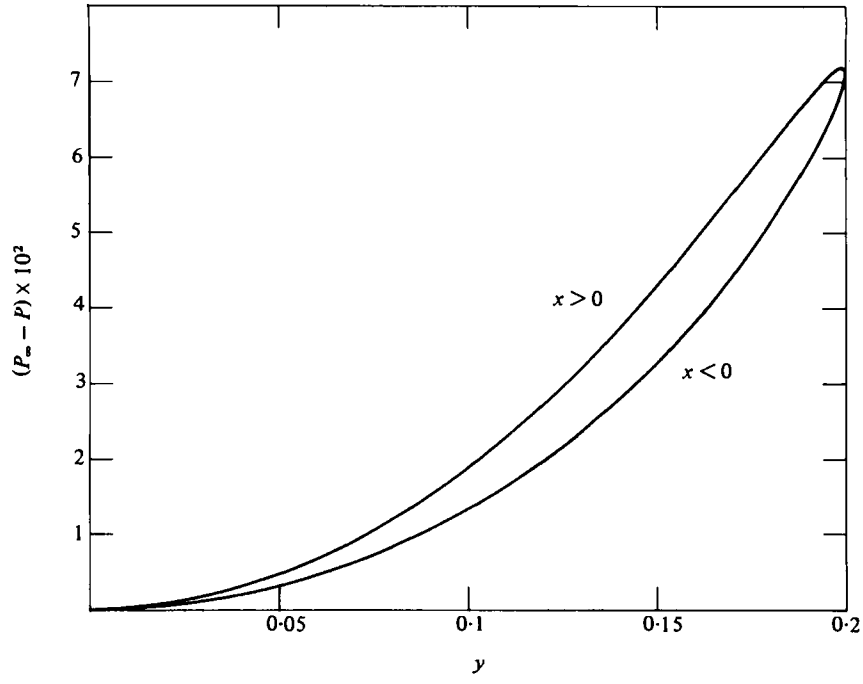

FIGURE 5. The pressure on the surface of the semicircle as a function of y for the case $F = 0{\cdot}5$, $\alpha = 0{\cdot}2$.

$F = 0{\cdot}5$. The linearized drag, calculated from (3.7), is compared with the drag obtained from the nonlinear solution, using (2.13). The linearized and nonlinear results agree well until a circle radius of about 0·12 is reached. Thereafter, nonlinear effects dominate, producing a force on the semicircle which is well in excess of the predictions of linearized theory.

The pressure on the surface of the circle for the nonlinear solution is shown as a function of y in figure 5, for the case considered in figure 3. To show more clearly the differences between the pressure distributions on the upstream and downstream portions of the semicircle, the pressure has been subtracted from the reference value

$$P_\infty = -2\frac{F^2}{\alpha^2}(\alpha^2 - x^2) - (\alpha^2 - x^2)^{\frac{1}{2}} + 1 + \tfrac{1}{2}F^2,$$

which is the pressure that would be observed on the surface of the semicircle if the streamline $\psi = 1$ had the same shape as is obtained for two-dimensional potential flow about a circle in an infinite fluid ($f = 2\zeta$). Since P_∞ is symmetric about $x = 0$, it makes no contribution to the wave drag D, which is therefore the area enclosed by the curve in figure 5.

In figure 6, the wave drag is shown as a function of F, when $\alpha = 0{\cdot}1$. For low values of the Froude number, the linearized and nonlinear results are in good agreement, but this agreement becomes steadily worse as the Froude number is brought closer to the critical value $F = 1$. Note that the linearized drag has the limiting behaviour

$$D \to \tfrac{3}{2}\pi^2\alpha^4 \quad \text{as} \quad F \to 1,$$

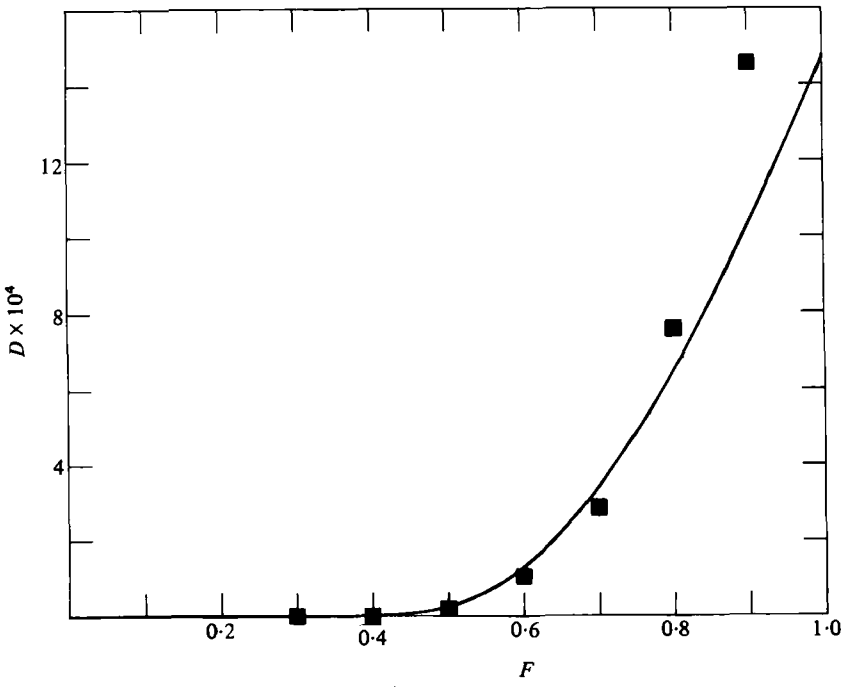

FIGURE 6. The dependence of wave drag upon F for the linearized (——) and nonlinear (■) solutions, when $\alpha = 0{\cdot}1$.

even although the linearized wavelength and wave height become infinite at this value of the Froude number.

The region of the parameter space in which we have been able to calculate nonlinear solutions possessing downstream waves is displayed in figure 7. The highest values of α for which the Newton process converged are marked on the diagram, for a range of different Froude numbers.

Although our numerical method has so far failed to yield a converged nonlinear solution for $F = 1$, it seems clear that such solutions should exist, since the free-surface profile is dominated by the Stokes waves which are formed downstream of the semicircle. The dashed line in figure 7 indicates the approximate position of the boundary of the region within which we conjecture the existence of solutions possessing a train of downstream Stokes waves. Note that this region extends well into the supercritical regime $F > 1$, terminating at $F = 1{\cdot}286$, which is Yamada's (1957) result for the highest solitary wave (indicated with a dotted line in figure 7). The portion of the dashed line lying in the region $F < 1$ was obtained from our numerical results by extrapolating plots of wave height *versus* α^2 up to the maximum wave height for Stokes waves computed by Schwartz (1974) and Cokelet (1977).

5.2. *Supercritical case*, $F > 1$

In the linearized theory, the critical value $F = 1$ is associated with the emergence of a fundamentally different type of solution, symmetric about $x = 0$ and possessing no waves. The nonlinear results confirm the existence of such a solution. Despite its appearance, this solution bears no relation to the solitary wave, since it reduces to uniform flow as $\alpha \to 0$.

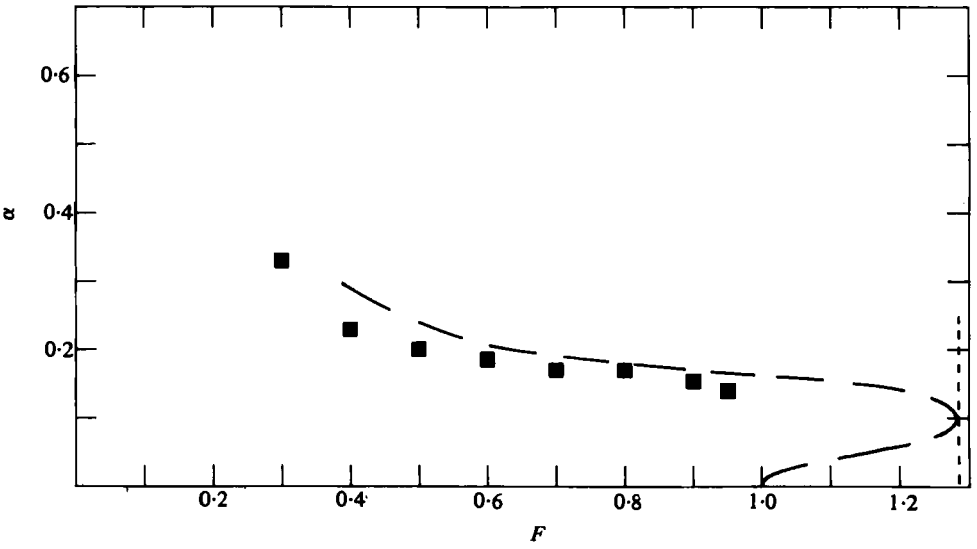

FIGURE 7. The region in the parameter space in which nonlinear wave-like solutions may be obtained. The points indicate the highest values of α for which Newton's method converged, and the dashed line is the boundary of the region in which solutions are conjectured to exist. The dotted line is Yamada's (1957) result for the highest solitary wave.

The region of the parameter space in which these nonlinear wave-free solutions may be calculated is again restricted, as is shown in figure 8. We have marked on this figure the largest values of α for which the Newton process converged, for a range of different Froude numbers. Our numerical results suggest that, like the linearized solution, the nonlinear wave-free solution exists only for $F > 1$. Nonlinear solutions may be obtained in the region to the right of the points marked on the diagram.

The physical mechanism which restricts the nonlinear solution to only a portion of the parameter space is apparently the formation of a sharp crest at the surface, with an included angle of 120°, exactly as in the case of Stokes waves. Indeed, Stokes' (1880) original analysis is local to the crest, and takes no account of whether or not the rest of the fluid contains waves.

The dashed line in figure 8 is the approximate position of the boundary of the region in which nonlinear, wave-free solutions are expected to exist. Solutions for which the parameters F and α describe a point on this line will possess a free surface containing a sharp crest where the fluid is at rest at the maximum height $y_{\max} = 1 + \frac{1}{2}F^2$. This dashed line has been obtained from our numerical results by extrapolating plots of maximum free surface elevation *versus* α^2 up to the height $y_{\max}$ at which the crest occurs.

In figure 9 we present nonlinear solutions for $F = 2{\cdot}1$, for three different values of the circle radius α. The value $\alpha = 1{\cdot}32$ is the largest circle radius for which Newton's method converged at this value of the Froude number. Also shown on this figure is a portion of the conjectured limiting profile, containing a sharp crest with sides that enclose an angle of 120°. Of course, our existing numerical technique is not capable of resolving a region of such high curvature, but it is possible that this difficulty may be overcome by spacing points unevenly at the free surface.

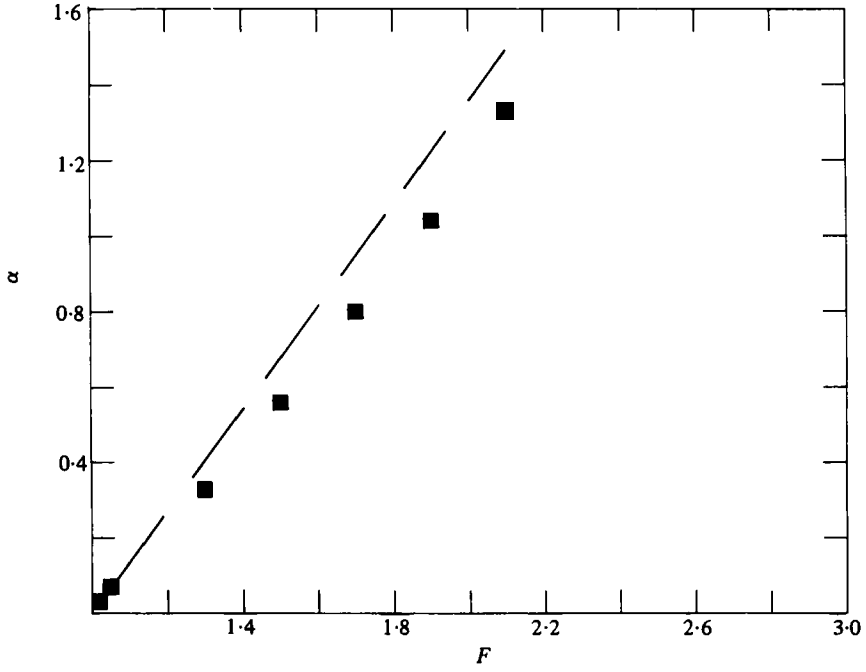

FIGURE 8. The region in the parameter space in which nonlinear wave-free solutions may be obtained. The points indicate the highest values of α for which Newton's method converged, and the dashed line is the boundary of the region in which solutions are conjectured to exist.

6. Summary and discussion

Two-dimensional fluid flow over a submerged semicircle has been investigated. The solution is facilitated by the choice of the complex potential f, rather than physical plane co-ordinates, as the independent variable.

A linearized solution has been developed by retaining the first term of a regular series expansion in the square of the circle radius, α^2. For subcritical flow, $F < 1$, a wave-free region is predicted upstream, followed by a regular wave train downstream. For $F > 1$, a symmetric wave-free solution is predicted. There is no solution for $F = 1$.

The exact nonlinear equations are solved numerically at the free surface by a process of Newtonian iteration. In the subcritical case, $F < 1$, an essentially wave-free region is obtained upstream followed by a train of nonlinear Stokes waves downstream. A comparison of the downstream waves obtained by our method with a train of Stokes waves confirms the accuracy of our method. In addition, the accuracy of our results is checked by observing that the solutions obtained are scarcely affected by further reduction in the numerical point spacing. However, due to the relatively small number of free-surface points to which we are restricted, we are unable to compute the very steep waves obtained when α is large or F is close to one. When α is large, the linearized theory severely underpredicts the value of the drag force on the semicircle, indicating the importance of nonlinear effects in these cases.

In the supercritical case, $F > 1$, the symmetric, wave-free profile predicted by the linearized solution is confirmed by the nonlinear results, although its physical existence seems implausible. It appears that the nonlinear free-surface profile is ultimately limited by the formation of a sharp crest with sides that enclose an angle of 120°.

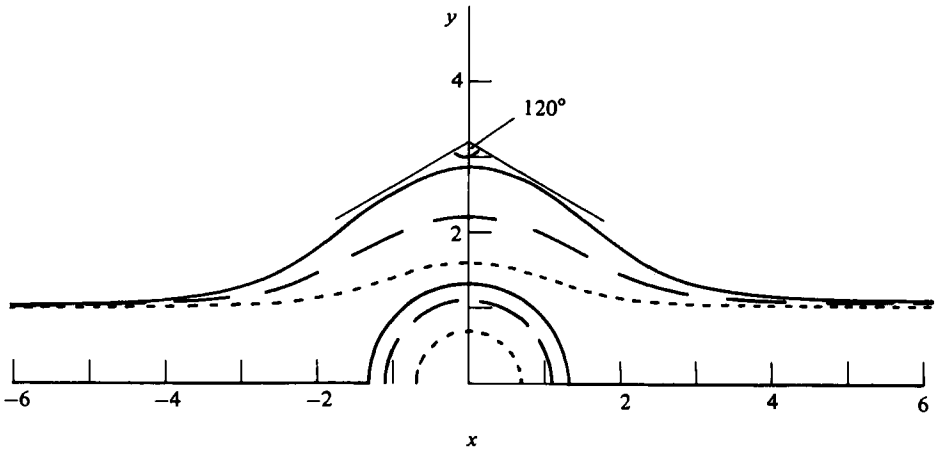

FIGURE 9. Nonlinear solutions for $F = 2{\cdot}1$, and $\alpha = 0{\cdot}7$ (· · · · · ·), $1{\cdot}1$ (— —), $1{\cdot}32$ (——). A portion of the conjectured limiting profile with a 120° angle at the crest is also shown. The fluid is flowing from left to right.

Although we have so far been unable numerically to obtain nonlinear wave-like solutions for $F = 1$, there seems no particular reason to doubt their existence at this and higher values of the Froude number, since it is well known that finite-amplitude Stokes waves can exist for Froude numbers either side of unity. Indeed, we expect that by employing more accurate techniques and a more sophisticated Newton iteration routine, these hitherto inaccessible regions of the solution space will become available to us. It would therefore appear that in a portion of the supercritical flow regime, $F > 1$, there exists a lack of uniqueness in the solutions to this problem, since both the symmetric wave-free solution and a solution containing a train of Stokes waves downstream must be considered as possible outcomes.

This work was supported by an Australian Commonwealth Postgraduate Research Award.

REFERENCES

COKELET, E. D. 1977 Steep gravity waves in water of arbitrary uniform depth. *Phil. Trans. R. Soc. Lond.* A **286**, 183–230.

GAZDAR, A. S. 1973 Generation of waves of small amplitude by an obstacle placed on the bottom of a running stream. *J. Phys. Soc. Japan* **34**, 530–538.

HAUSSLING, H. J. & COLEMAN, R. M. 1977 Finite-difference computations using boundary-fitted coordinates for free-surface potential flows generated by submerged bodies. In *Proc. 2nd Int. Conf. on Numerical Ship Hydrodynamics, Berkeley*. pp. 221–233.

HAVELOCK, T. H. 1927 The method of images in some problems of surface waves. *Proc. R. Soc. Lond.* A **115**, 268–280.

KOCHIN, N. E., KIBEL', I. A. & ROZE, N. V. 1964 *Theoretical Hydromechanics*. Wiley-Interscience.

LAMB, H. 1932 *Hydrodynamics*, 6th edn. Cambridge University Press.

SCHWARTZ, L. W. 1974 Computer extension and analytic continuation of Stokes' expansion for gravity waves. *J. Fluid Mech.* **62**, 553–578.

SCHWARTZ, L. W. & VANDEN-BROECK, J.-M. 1979 Numerical solution of the exact equations for capillary-gravity waves. *J. Fluid Mech.* **95**, 119–139.

SHANKS, S. P. & THOMPSON, J. F. 1977 Numerical solution of the Navier–Stokes equations for 2D hydrofoils in or below a free surface. In *Proc. 2nd Int. Conf. on Numerical Ship Hydrodynamics, Berkeley*. pp. 202–220.

STOKES, G. G. 1880 *Mathematical and Physical Papers*, vol. 1. Cambridge University Press.

TUCK, E. O. 1965 The effect of non-linearity at the free surface on flow past a submerged cylinder. *J. Fluid Mech.* **22**, 401–414.

VON KERCZEK, C. & SALVESEN, N. 1977 Non-linear free-surface effects – the dependence on Froude number. *Proc. 2nd Int. Conf. on Numerical Ship Hydrodynamics, Berkeley*. pp. 292–300.

WEHAUSEN, J. V. & LAITONE, E. V. 1960 Surface waves. In *Handbuch der Physik*, vol. 9. Springer.

YAMADA, H. 1957 On the highest solitary wave. *Rep. Res. Inst. for Appl. Mech., Kyushu University* no. 5, pp. 53–67.